Central European Journal of Energetic Materials
ISSN 1733-7178; e-ISSN 2353-1843

Cent. Eur. J. Energ. Mater. 2022, *19*(1): 63-90; DOI 10.22211/cejem/147682
Article is available in PDF-format, in colour, at:
https://ipo.lukasiewicz.gov.pl/wydawnictwa/cejem-woluminy/vol-19-nr-1/

Research paper

Influence of Liner Wall Thickness on the Penetration Performance of PETN-HTPB PBX-based Shaped Charges into Steel Targets

Tamer Elshenawy[1,*)], Eldesoky Ezzat[2)], Ahmed M. Riad[2)], Mohamed Abd Elkader[2)]

[1)] *Technical Research Centre, Cairo, Egypt*
[2)] *Military Technical College, Egyptian Armed Forces, Kobry Elkobbah, 11765, Egypt*
**E-mail:* tamershenawy@yahoo.com

ORCID Information
Elshenawy T.: https://orcid.org/0000-0002-9934-9178

Abstract: The thickness of a shaped charge liner is one of the essential parameters that must be considered when optimizing penetration depth into a target material. In this paper, experimental and analytical studies have been implemented using shaped charges having copper liner thicknesses ranging from 0.7 to 1.3 mm in an optimization study of the influence of jet characteristics on the achieved penetration depths into steel targets. The shaped charges were filled with equal masses of PETN-polyurethane based PBX explosive charges and fired against steel targets placed at 29 mm stand-off distance. The experimental measurements show that the depth of jet penetration into steel targets increased with liner thickness up to a thickness of 1.1 mm, after which the penetration decreased again. A numerical study was also carried out using the hydrocode Autodyn to model the jets used in the optimization analysis, which accounted for the variation of penetration depth using different liner thicknesses. This analysis also showed why the penetration depth achieved with a liner thickness of 1.0 mm was not optimum due to its non-coherent formed jet. Instead, a liner with a wall thickness of 1.1 mm exhibited the optimum penetration depth of 12.8 cm.

Keywords: shaped charges, Autodyn jetting, steel target, liner thickness, jet penetration

1 Introduction

Shaped charges consist of a confined cylinder explosive charge containing a cavity lined with a ductile metal such as OFHC copper at one end and a detonator at the opposite end. Based on the explosive type initiated by the detonator, a detonation wave starts to propagate within the explosive at a velocity of about 9 km/s [1]. When the detonation wave strikes the liner, it starts to collapse by flowing towards the charge's centerline under a high pressure loading. Part of the collapsed liner material forms a jet that moves with a high tip velocity (7-9 km/s) [2, 3]. The jet so formed elongates due to the existence of a velocity gradient along its length. The stand-off distance between the charge base and the target surface allows the jet to elongate until either it is completely consumed during penetration or it breaks up into small fragments. A continuous long jet is capable of achieving a large penetration depth into the target material depending on its solid state and porosity [4]. The penetration is mainly caused by the lateral displacement of target material due to the pressure generated by the impacting jet, which is very high compared with the strength of the target material [1].

Much research has been performed to investigate the effect of explosive-liner mass ratio, explosive type and the effect of liner thickness on the jet formation process and its subsequent penetration potential into monolithic targets and various alloy material targets [5].

Nan *et. al* [6] investigated experimentally and numerically the penetration performance of shaped charges composed of three different types of explosives, namely RDX, HMX and CL-20. They performed cylinder expansion tests to estimate the JWL parameters and the Gurney velocity for each explosive that they studied. The JWL equation of state was used in Autodyn hydrocode to model the studied explosives. The results they obtained for shaped charges loaded with CL-20 based explosives achieved respectively 17 and 3% higher penetration depths into steel targets than those loaded with RDX- and HMX-based explosives. They attributed the higher penetration of shaped charges containing CL-20 to its higher velocity of detonation, C-J pressure and Gurney constant compared with the other two explosives.

Saran *et. al* [7] experimentally investigated the performance of shaped charges with liners of various shapes (conical, trumpet) manufactured out of different aluminum alloys of three different thicknesses (4, 6 and 8% of the

charge diameter (CD)). The aluminum alloys they used were in the 5000, 6000 and 7000 series. They tested the shaped charges against both sand and SAE 1020 steel targets. The set of the tested charges was located either at a moderate stand-off distance (3 CD) or large (15 CD). They found that liners of small thickness penetrated deeper but with slightly smaller crater diameters (*e.g.* conical shaped charges with liner wall thicknesses of 4, 6 and 8% of CD achieved penetration depths of 2.41, 1.46 and 1.13 CD into steel targets, respectively, when fired at a stand-off distance of 15 CD.

Dehestani *et al.* [8] also studied the effect of stand-off distance and liner thickness on the penetration performance of shaped charge jets. Their simulated liners had conical shapes with a charge diameter of 30.2 mm and liner thicknesses of 0.5, 0.6, 0.8, 1.0, 1.2, 1.4 and 1.6 mm. For each liner thickness, both the jet formation process and its penetration into AISI 1045 steel target were predicted using ABAQUS finite element software. They validated their predicted penetration depths with experimental firings of some shaped charges having liners with various wall thickness. The results they obtained showed that decreasing the liner thickness from 1.6 to 0.6 mm increases the jet tip velocity, which in turn increases the penetration depth from 40 to 65 mm as shown in Figure 1. On the other hand, a shaped charge with a liner wall thickness of 0.5 mm achieved a penetration depth of only 63.9 mm, which may be attributed to the jet breaking up before starting to penetrate the target. This means that if the liner wall thickness is decreased below a certain critical value, the penetration potential begins to decrease again. This means that an optimization study has to be performed to determine the optimum liner wall thickness.

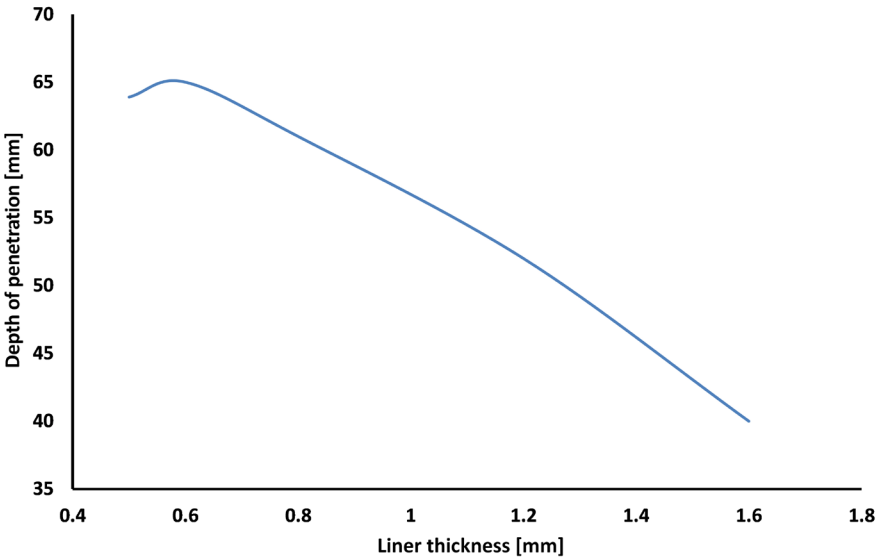

Figure 1. Plot of the dependence of jet penetration depth on liner wall thickness (data taken from [8])

Using the LS-DYNA code, Ou *et al.* [9] numerically studied the effect of the design parameters of a shaped charge on its penetration process. The parameters they studied were the cone apex angle, the liner wall thickness, the stand-off distance and the detonation point. Each design parameter was investigated individually. They used the Taguchi method to evaluate the effectiveness of each parameter by identifying its signal to noise ratio. Then they predicted the optimal parameter level using statistical equations. Their analysis showed that the design parameter with the most effect was the initiation point which contributed about 23% of the predicted penetrated depth, whereas the liner wall thickness had only an 11% effect of the depth of penetration. Figure 2 is a plot of the predicted penetration depths of jets formed from liner thicknesses of 0.05, 0.75, 1.05, 1.35 and 1.6 mm (*i.e.* 0.7 to 2.3% of the CD) based on the data retrieved from [9].

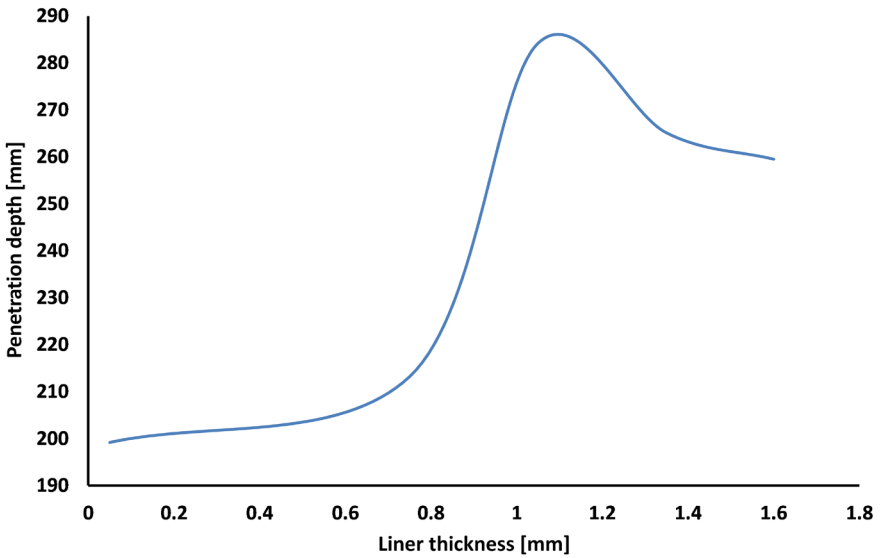

Figure 2. Plot of the jet penetration depth with liner wall thickness (data taken from [9])

It can be concluded from the research published in Refs. [7-9] that there is evidence of an effect of liner wall thickness on the performance of shaped charges in terms of their jet mass and velocity as well as the penetration depths achieved into different targets.

In the present research, an experimental program was conducted to test a few manufactured small size shaped charges loaded with the same amount of PETN-based polyurethane PBX charges. These shaped charges were tested against steel targets in order to investigate the effect of different copper liner wall thicknesses on the jet penetration depths. The Autodyn hydro-code was also used to simulate the tested shaped charges with different liner thicknesses so as to predict the main parameters associated with jet formation and its penetration potential into steel targets. Moreover, based on the extensive jetting analysis results obtained using the Autodyn hydrocode, jet breakup times and penetration depths were predicted for all the shaped charges tested, allowing the optimized liner wall thickness to be selected and then tested experimentally.

2 Experimental Work

2.1 General information

An experimental program was conducted to manufacture PETN-polyurethane based PBX explosive and to assemble small size shaped charges with different liner wall thicknesses and to test their penetration potential into steel targets. In what follows, the manufacturing techniques for both the liner and the explosive are presented together with the charge assembly and field testing.

2.2 The liner

The liners were made of Oxygen Free Electrolytic Copper (OFEC) sheet with a high purity of 99.99% Cu. This material has very low oxygen and phosphorus contents giving it the high ductility needed for the jet material to sustain a long break-up time and a better cohesive performance [10]. The copper liners were manufactured using a shear forming technique, which starts with cutting circular copper discs which are then annealed at 400 °C for 30 min prior to plastic deformation to decrease the strain hardening and to maintain the material ductility during the flow forming process [11]. The manufactured copper liners had a trumpet shape with a base diameter of 33 mm and uniform liner wall thicknesses. The liner wall thicknesses used were 0.8, 0.9, 1.0, 1.1 and 1.2 mm.

2.3 The explosive charge

The explosive charges that were used were a cast cured plastic bonded explosive (PBX) based on PETN and polyurethane with a total average mass of 40.0 g. The PETN main powder was bimodal with the coarse crystals having an average particle size ranging from 150 to 200 μm and the fine crystals being about 38 μm in size. This powder was produced by Anjana Explosives Ltd. (India). An inert thermoset binder hydroxyl terminated poly butadiene (HTPB) with a 0.78 NCO/OH ratio cured using hexamethylene diisocyanate (HMDI) obtained from Shandong Yucheng Yiao Technology Co. Ltd. (China) was also used in the formulation. Dioctyl azelate (DOZ) was used as a plasticizer to decrease the viscosity of the mixture and make the mixing and casting process easier. The formulation was processed using a cast cured technique (solvent-less technique), in which the polymeric binder (HTPB), plasticizer (DOZ) and MAPO were transferred under vacuum using a vertical stainless steel mixer at 60 °C for 7 min to ensure uniform distribution. The PETN powder was then added in small portions 2-3 times during mixing without vacuum at 60 °C for 2-3 h. The mixing operation then continued for 30 min under vacuum at 60 °C to ensure complete coating of the explosive grains after complete addition of the high explosive. Then the temperature

of the mixture was cooled down to 40 °C, the HMDI was then added and then mixed for about 25 min to obtain a uniform dough. 40.0 g of the dough was then cast into each shaped charge steel case, after which the liner was inserted manually in an upright position inside the charge casing to make sure its axis coincided with that of the charge casing. Mild hydraulic pressing (15-20 MPa) was applied slowly allowing time for trapped air to escape. This avoids non-uniformity in the distribution of the explosive charge load which would result in a non-homogenous detonation velocity and unpredictable performance. These steps in the explosive-liner and casing assembly are shown in Figure 3. The charges filled with PETN-polyurethane based PBXs were then left to cure for 10-15 days at 55-60 °C. The formulation of the PETN-HTPB PBX we used is shown in Table 1. Theexperimental facilities of the Abo-Zabal Company for Chemical Industries (Egypt) were used for preparing this explosive type.

Table 1. Compositions of the prepared PETN based PBXs

Ingredient	PETN	HTPB	HMDI	DOZ	MAPO
Content [wt.%]	78	17.08	0.96	3.46	0.5

Figure 3. The explosive loading and the liner assembly (hydraulic pressing step not shown)

2.4 Density and detonation velocity measurements

The manufactured PETN-based PBX density was measured using the Laboratory Facilities of the Abou Zabal industrial factory and was found to be 1.45 g/cm^3. The detonation velocity of the PBX was measured using a hand-held detonation velocity tester Model VOD-812 produced by OZM Research (Pardubice, Czech Republic) [12]. The tested specimens were cut in the form of a sheet with 1 cm thickness, 2 cm width and 15 cm length. The time interval taken by the detonation wave to cover the distance between the start and the end fiber optic probes was measured, which gave the detonation velocity to high precision.

Each specimen type was tested three times, giving an average measured detonation velocity of 6970 m/s with a standard deviation of 45 m/s.

2.5 Calculation of the detonation characteristics

The theoretical detonation characteristics such as the detonation pressure and the heat of detonation of the manufactured PETN-based PBX explosive were calculated using the EXPLO5 thermodynamic code [13]. The BKW Equation of State (EOS) parameters were applied. The values of these parameters were:

– $\alpha = 0.5$,
– $\beta = 0.298$,
– $k = 10.50$, and
– $\Theta = 6620$.

The calculated detonation characteristics of the PETN-based PBX explosive showed that the detonation pressure was 17.2 GPa, and the detonation heat was 5268 J/g. The calculated detonation velocity was 6996 m/s, which was lower than the experimentally measured value by about 0.37%. This fact gives confidence in and verification of the used code. The JWL EOS coefficients relevant to our PETN-based PBX formulation composition were also calculated and are listed within the numerical material model section [14, 15].

2.6 The charge assembly and the static firing

Each manufactured tested liner was assembled with a casing made of 4340 steel. Then the same amount of explosive charge was loaded and a base detonator fastened to the end of the charge using the experimental facilities of the shaped charge laboratory of the Research Center of the Armed Forces (Cairo, Egypt). Five small size shaped charges with different liner thicknesses ranging from 0.8 up to 1.2 mm with an increment of 0.1 mm were prepared.

The selected target material was steel 52 grade consisting of laminated layers; each layer having a thickness of 25.4 mm. The layers of the steel target plates were welded together at their peripheries where the total thickness of the target was greater than the jet penetration depth of the shaped charges used. The hardness of the target material was measured using the laboratory facilities of the Cairo Research Center. Three measurements were recorded after grinding the target surface. The hardness was measured at different points on the surface of each specimen and their average values were found to be 195 HB with standard deviation of 3 HB. The measurements were carried out using an Ultrasonic Portable Hardness Tester Non-Destructive Model PHT-6000 series. Material bulk modulus and related mechanical properties were obtained using the matweb database [16].

The ballistic static firing of the prepared shaped charges was carried out in the shooting range of the Cairo Research Center. The ballistic set-up consisted mainly of:

– detonator,
– power supply,
– prepared shaped charge, and
– laminated steel target.

The steel target was placed at a stand-off distance of 29 mm below the tested charge. A photograph of the ballistic set-up is shown in Figure 4. For each tested shaped charge, the ballistic measurements were mainly concerned only with the depth of jet penetration into the steel target and the crater shape inside this target material. These measurements were made after cutting longtudinal half sections of the formed craters using a vibrator saw.

Figure 4. Ballistic test setup of the constructed shaped charges and the testing facility

3 Numerical Simulation

3.1 General information

An Autodyn-2D numerical hydrocode was used to investigate the influence of shaped charge liner wall thickness on the relevant jet characteristics and their impact on the penetration depths achieved into steel targets. Descriptions of the

shaped charge elements, their material models consisting of their equations of state and strength models, are introduced briefly. Moreover, a mesh sensitivity analysis study was also performed in order to investigate the effect of mesh size on the produced jet characeristics and relevant jetting parameters.

3.2 Material models for the shaped charge elements and the steel target

The equation of state for the 4340 steel casing was selected to be linear whereas the initial elastic behavior was expressed by Hooke's Law [17]. The casing material used had a density of 7.83 g/cm^3 and a bulk modulous of 160 GPa. The adopted strength model used for the 4340 steel was Johnson-Cook (J-C) [18]. The J-C parameters were:

– the yield strength A = 792 MPa,
– the strain-rate constant B = 510 MPa, the hardening exponent n = 0.26, the strain-rate constant C = 0.014, the thermal exponent constant; m = 1.03 and the normalized effective plastic strain-rate = 1.

The OFHC copper liner material with a density of 8.93 g/cm^3 was modeled by the shock equation of state with sound speed value (C_o) of 3940 m/s, slope value (S) of 1.489 and reference temperature of 293 K. The adopted strength model was J-C [18]. The J-C parameters were:

– the yield strength A = 90 MPa,
– the strain-rate constant B = 292 MPa,
– the hardening exponent n = 0.31,
– the strain-rate constant C = 0.025,
– the thermal exponent constant m = 1.09, and
– the normalized effective plastic strain-rate = 1.

Interested readers should consult Ref. [18] for a detailed explanation and discussion of the J-C model and its modifications (J-C-M) [19].

The EOS for the high explosive employed was the Jones-Wilkins-Lee (JWL) equation. For the explosive used, experimental constants were determined from sideways plate push dynamic test experiments [20] and the cylinder expansion test [21-23]. The PBX explosive loading density was 1.45 g/cm^3. Parameters in the JWL EOS were:

– $A = 6.098 \cdot 10^8$ kPa,
– $B = 1.298 \cdot 10^7$ kPa,
– R_1 = 4.5,
– R_2 = 1.4, and
– ω = 0.25.

In addition, the measured detonation velocity of 6970 m/s, the detonation pressure

of 17.2 GPa and C-J energy per unit volume of $7.6386 \cdot 10^6$ kJ/m^3 were fed into the code.

The equation of state for the steel target material was selected to be linear with a density of 7.83 g/cm^3 and a bulk modulus of $1.6 \cdot 10^8$ kPa [16]. The strength model was neglected because of the tremendous stagnation pressure generated during the jet-target interaction [1].

3.2 Numerical algorithms of shaped charge

3.2.1 Jetting analysis algorithm

The standard jetting analysis, the jet formation and its penetration algorithms are the two main algorithms used in the Autodyn hydrocode. Detailed descriptions of these algorithms are reported in [2]. The jetting analysis is the simplest process that predicts the parameters associated with the jet formation process; *i.e.* during the liner collapse until the jet is formed. Jetting analysis calculations are based on the Pugh-Eichelberger-Rostoker (PER) theory of jet formation [24, 25]. Figure 5 illustrates the constructed shaped charge including the 4340 steel case, the explosive and the trumpet liner with fixed apex node. This is considered to be a complete representation of the jetting analysis process in the Autodyn hydrocode. The main steps used to simulate the jetting analysis process are reported in [3, 26, 27].

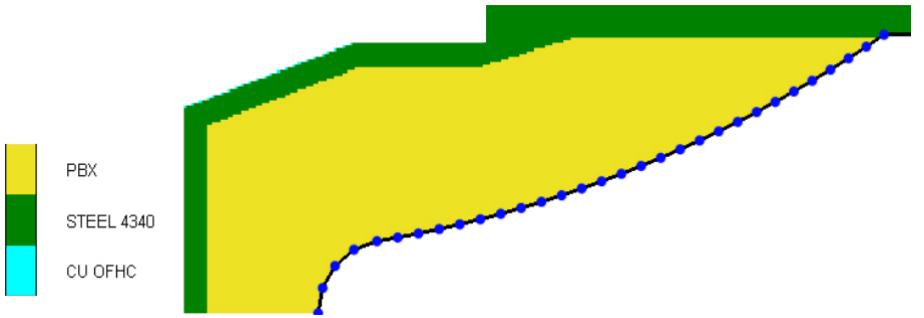

Figure 5. Initial model of the jetting analysis process

3.2.2 Jet formation and penetration algorithm

The jet formation process shows the profile of the formed jet as a function of time, in addition to the contours of different jet parameters, the jet break-up and its particulation phenomena. The cut-off velocity was also determined using this algorithm when the target material was added to the jet within the same part.

The jet is allowed to penetrate the target material as deep as it can, while the cut-off velocity is identified as the point when the penetration progress stops. In addition, the performance of the formed jet, which is strongly affected by the detonation wave front incident upon the liner surface, can also be shown in this algorithm. The initiation method, which affects the detonation wave shape and the associated pressure, was also considered as one of the factors influencing the shaped charge performance using this jet formation algorithm. The complete procedures for simulating the jet formation process and describing the initiation point for the explosive charge are reported in [3, 17].

3.3 Mesh sensitivity

It is known that the mesh size and its shape affect the accuracy of the numerical results obtained [28, 29]. Using a fine mesh gives accurate results, but it takes much more time than if a coarse mesh is used. The mesh sensitivity study was performed for the jetting analysis algorithm so as to study the sensitivity of the characteristics of the jet produced (such as jet mass, velocity and kinetic energy) to the initial mesh size used. In this sensitivity study, a Euler common space of both explosive charge and steel casing was represented in the algorithm by grids with uniform square cell sizes. The jetting model was run until complete jetting was obtained using 10 different mesh sizes of 0.5, 0.33, 0.25, 0.2, 0.167, 0.142, 0.125, 0.111, 0.09 and 0.077 mm. The output data were assembled after terminating the jetting analysis trial, in which all the liner elements were collapsed and directed towards the charge axis forming both a jet and a slug. A summary of the used mesh sizes and relevant jet characteristics is presented in Table 2 and shown in Figure 6 as an example for the convergence of the solution to a steady jet mass at a value of 3.05 g for a shaped charge with a liner thickness of 1 mm.

Table 2. Predicted jet mass using different mesh sizes for shaped charges with a liner thickness of 1 mm

Lines [mm]	2	3	4	5	6	7	8	9	11	13
Mesh size [mm]	0.5	0.33	0. 25	0.2	0.167	0.142	0.125	0.111	0.09	0.007
Jet mass [g]	3.573	3.204	3.450	3.005	3.205	2.980	3.050	3.019	3.002	2.997
Time consumption [min]	5	10	20	35	60	90	140	200	350	580

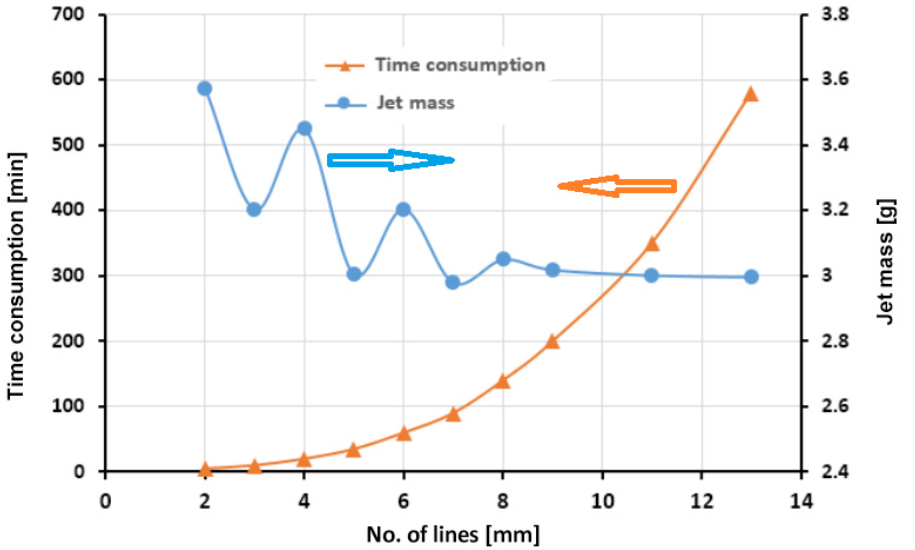

Figure 6. Jet mass and time consumption versus mesh size for shaped charge with a liner thickness of 1 mm

Based on Table 2 and Figure 6, there is a mild dependence of the calculated jet mass on the mesh size used, but the dependence is crucial when the calculation time is also considered. The calculation time is an essential parameter and it could not be neglected in this study as it is almost an exponential function of the mesh size used. A mesh size of 0.125×0.125 mm predicted an increase in jet mass of about 0.053 g compared with a calculation performed using a mesh size of 0.007×0.007 mm; *i.e.* it increased by about 1.76%. Moreover, the time saved in running the program using a mesh size of 0.125×0.125 mm was about 440 min compared to when a mesh size of 0.007×0.007 mm was used. Therefore, a mesh size of 0.125×0.125 mm was selected for the rest of the calculations due to its affordable calculation time.

To show the area of the liner material affected by performing jetting analysis with different mesh sizes, Figure 7 plots the dependence of cumulative jet mass with relative axial distance from the liner apex. The figure shows that near the apex of the liner, a common behavior is obtained with very similar cumulative jet masses, but differences due to the different mesh sizes begin to occur at about 80% of the relative axial distance from the apex. This means closer to the liner base, the greater the percentage of the liner mass that flows inwards to form the jet. The overall convergence was shown to be above 90% for the finest mesh of 0.007×0.007 mm.

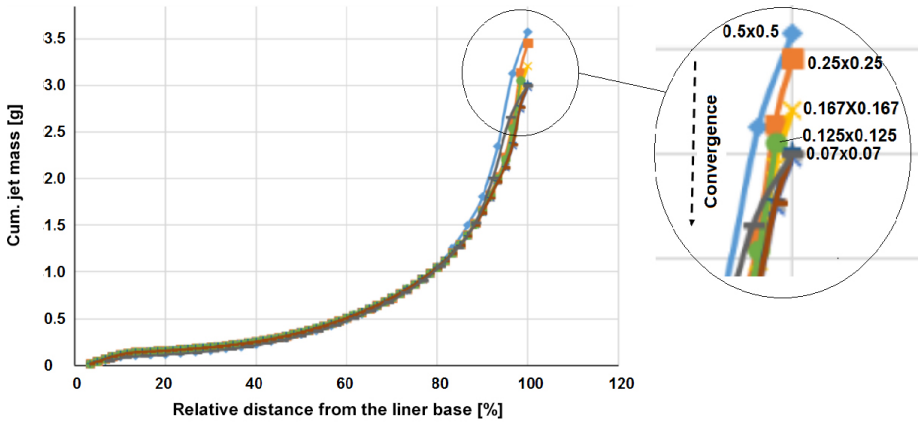

Figure 7. Cumulative jet mass versus jet axial coordinate obtained from the jetting analysis using different mesh sizes for a shaped charge with a liner thickness of 1 mm

4 Results and Discussion

4.1 Jetting analysis results

The liner thickness has a great influence on jet formation and penetration process. It affects the jet velocity and its mass affecting jet penetration since it is directly proportional to jet momentum and relevant kinetic energy. Table 3 lists the jetting analysis results including jet velocity, momentum and relevant kinetic energy for each shaped charge with liner wall thickness ranging from 0.7 to 1.3 mm.

It can be seen from Table 3 that both the jet mass and momentum increase with increasing liner wall thickness. On the other hand, both the jet tip velocity and associated kinetic energy behave differently as they decrease with increasing liner wall thickness.

Because jet penetration into the target depends mainly on the jet mass and its kinetic energy, it is necessary to find the shaped charge design that gives optimum penetration performance. A simple 2-D optimization problem is presented in Figure 8 with the real limits of jet mass ranging from 2.31 to 3.59 g and jet kinetic energy (K.E.) ranging from 43.11 to 48.52 kJ. The two lines cross at a liner wall thickness of 1.05 mm which is the shaped charge liner wall thickness that gives the optimum depth of penetration into target. A more sophisticated optimization study is presented and discussed in Section 4.4.

Table 3. Jet masses, velocities, momentum and K.E. for different liner thicknesses

Liner thickness [mm]	Output					
	Liner mass [g]	Jet mass [g]	Ratio of jet mass to liner mass [%]	Jet tip velocity [m/s]	Jet momentum [kg·m/s]	Jet K.E. [kJ]
0.7	13.45	2.31	17.17	8776	13.988	48.52
0.8	15.38	2.55	16.60	8393	14.499	47.89
0.9	17.29	2.79	16.19	8290	14.874	47.20
1.0	19.22	3.05	15.60	8170	15.287	46.62
1.1	21.08	3.18	15.10	8120	15.576	45.83
1.2	23.00	3.40	14.78	7870	15.788	44.80
1.3	24.92	3.59	14.40	7656	16.005	43.11

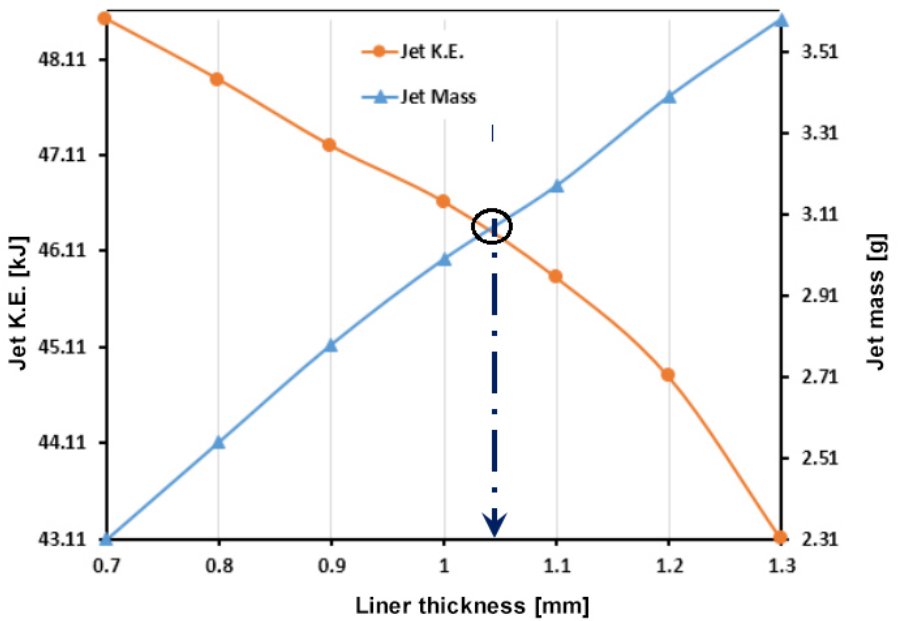

Figure 8. Prediction of liner wall thickness of 1.05 mm that gives the optimum penetration depth into target

A sample of the unsteady PER theory results based on the standard Autodyn jetting analysis algorithm is presented. The predicted change of jet tip velocity with cumulative jet mass for different liner wall thicknesses is plotted in Figure 9 for liner wall thicknesses of 0.9, 1.0, 1.1 and 1.2 mm. For each liner

wall thickness, the jet velocity obtained from the standard jetting analysis at the tip area is corrected based on the formula suggested by Chou and Flis [30] and verified by Gürel [28] considering the inverse velocity gradient near the apex region.

The present figure gives the same trends as those obtained analytically using the BASC code for the studied Aseltine shaped charge with a charge diameter of 81.3 mm and emphasized by X-ray trials [31]. The present figure confirms the validity and verification of the PER based jetting model, in which the jet velocities will be used for further analytical penetration calculations.

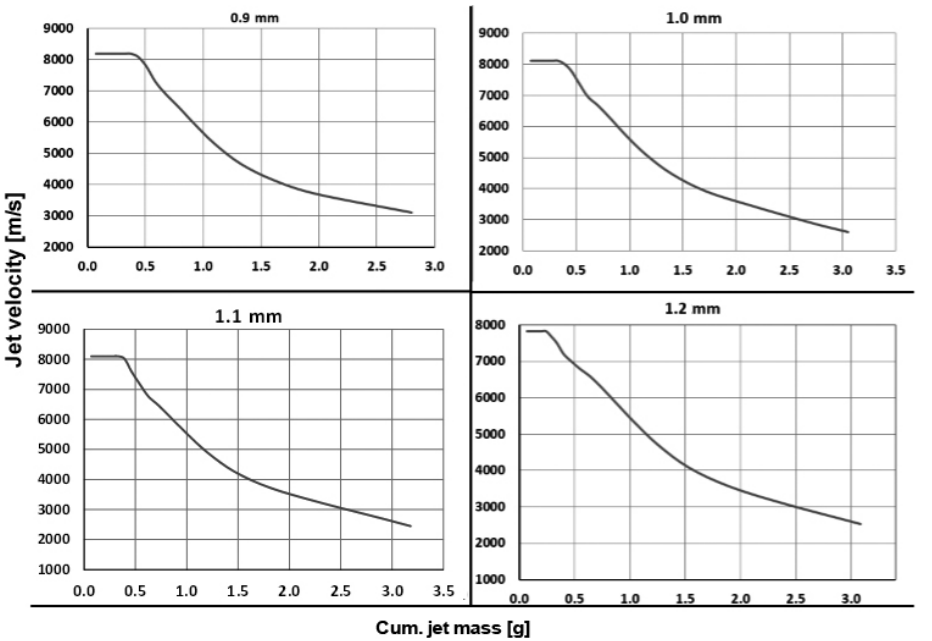

Figure 9. The jet tip velocities as function of cumulative jet mass for different liner wall thicknesses according to a standard jetting analysis algorithm

4.2 Breakup time

In addition to the numerical standard jetting analysis based on unsteady PER theory, other parameters should be examined in order to determine the best shaped charge w.r.t. penetration performance. These parameters include post-numerical analytical work that determines the jet breakup time and its penetration depth into a steel target. Hirsch [31] estimated the breakup time (t_b) of a jet element using Equation 1:

$$t_b = \frac{2r}{V_{PL}} \tag{1}$$

where r is the initial radius of the jet element when the jet forms, which can be measured using flash X-rays or estimated analytically using Equation 2:

$$r = \sqrt{2RT_L}\sin\left(\frac{\beta}{2}\right) \tag{2}$$

where R is the initial inner radius of the liner element, T_L is the thickness of the liner wall and β is the elemental collapse angle of the collapsed liner element calculated from jetting analysis (PER model) [25].

V_{PL} is a characteristic plastic velocity representing the average velocity difference between the neighbouring collapsed jet elements [32]. The reciprocal of V_{PL} (*i.e.* $1/V_{PL}$) represents the specific breakup time of copper [32] and zirconium jets [33]. For copper jets, the specific breakup time can be estimated using Equation 3:

$$\frac{1}{V_{PL}} = 13.886 - 101.149\left(\frac{T_L}{CD}\right). \tag{3}$$

For a given value of T_L/CD, the breakup time of the copper jet was estimated based on both scaled (T_L/CD) values and $1/V_{PL}$.

4.3 Prediction of penetration depth into steel target

Once the breakup time of the jet formed from each shaped charge studied has been estimated analytically, the penetration depth into a steel target is predicted based on the virtual origin model suggested by Allison and Vitali [34], discussed by DiPersio *et al.* [35] and summarized by Schwartz [36]. They presented three piecewise explicit functions that could be used to calculate the following:

– penetration before jet breakup,
– penetration when jet breaks up on entry into the target, and
– penetration when jet completely breaks up before reaching the target.

Further discussions and modifications of the virtual origin method are reported in [36].

It was found that the piecewise function conditions show that all the currently studied shaped charges starting from a liner thickness of 0.7 up to 1.3 mm undergo the second case penetration, in which jet breakup occurs during penetration into the target material. Therefore, the following equation was used to estimate the jet penetration depth into target [36].

$$P = \frac{(1+\gamma)(V_j t_b)^{\frac{1}{1+\gamma}} Z^{\frac{\gamma}{1+\gamma}} - (V_C t_b)}{\gamma} - Z_o \tag{4}$$

where P is the penetration depth into the target, γ is the ratio of the square root of target density to jet density, V_j is the jet tip velocity, t_b the average breakup time, V_C is the cut-off velocity and Z_o is the effective length of jet (*i.e.* the stand-off distance plus the distance from the virtual origin to the liner base). This length is bounded by Equation 5:

$$(V_C t_b)\left(\frac{(V_C}{(V_j}\right)^{\frac{1}{\gamma}} < Z_o < (V_j t_b) \tag{5}$$

Figure 10 shows the real representation of the back projection method applied for a liner thickness of 1.1 mm to determine the location of the virtual origin point allowing the effective jet length used in Equation 4 to be calculated. Z_o was determined using the same method reported in [29], where the shaped charge jet formation is used for further back projection to determine the location of the virtual origin point using two points. These two points are the stagnation point and the jet tip element. A sample of this relocation of the liner thickness of 1.1 mm is shown in Figure 10. Similarly, the same method has been implemented with the entire liner thickness to calculate the jet penetration analytically. The jet contours, the stretching shape and the time and axial distances for both the jet tip and the stagnation points were obtained using the shaped charge jet formation algorithm. The cut-off element velocity V_c was also determined by when jet penetration stops. The standard jetting analysis results obtained using the Autodyn hydrocode are listed in Table 4 together with the calculated breakup times and the penetration depths obtained using the virtual origin concept.

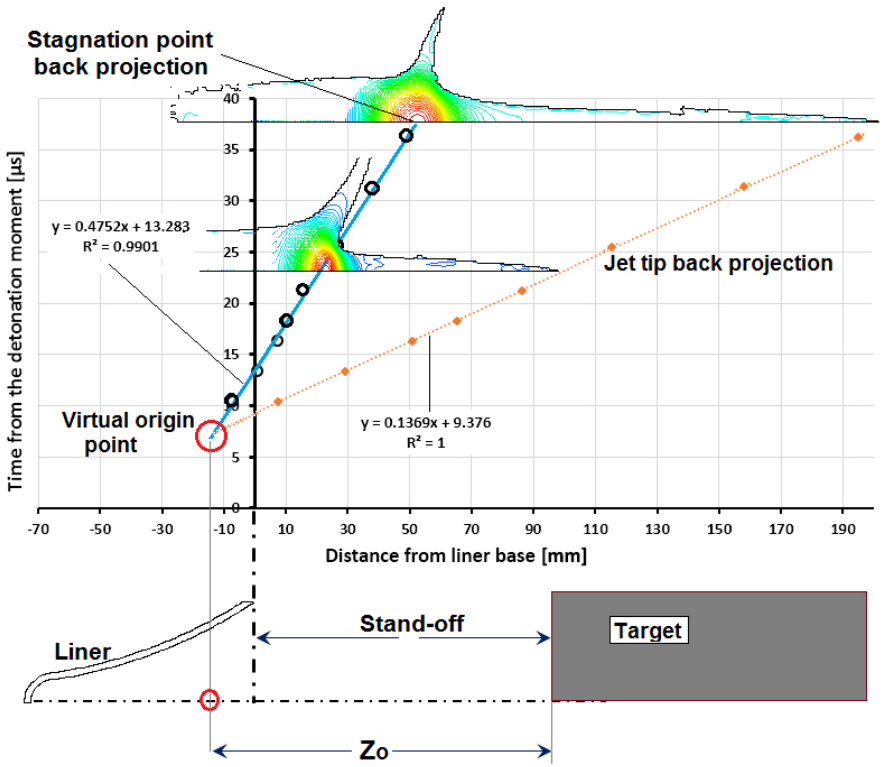

Figure 10. The back projection method used to determine the location of the virtual origin point and effective jet length for a 1.1 mm liner wall thickness

Table 4. Jetting analysis results obtained using Autodyn hydrocode, the calculated penetration depths were obtained by the virtual origin method and the corresponding measured depths of the shaped charges tested

T_L [mm]	V_j [m/s]	V_C [m/s]	Z_o [mm]	Average break-up time, $t_{b\,av.}$ [µs]	γ	Predicted P [mm]	Measured P, $P_{exp.}$ [mm]	Error [%]
0.7	8776	2283	44.0	18.17	0.934	88.88	–	–
0.8	8393	2050	43.5	19.79	0.934	93.14	82	–13.59
0.9	8290	1779	43.5	20.41	0.934	98.93	90	–9.93
1.0	8170	1622	42.5	21.33	0.934	103.00	98	–5.10
1.1	8120	1427	42.5	24.00	0.934	113.64	128	11.22
1.2	7870	1350	39.5	25.00	0.934	111.33	114	2.34
1.3	7656	1299	36.5	26.00	0.934	109.02	–	–

4.4 Optimization of the liner wall thickness results

The objective of this optimization study was to determine the optimum value of the liner thickness T_L, at which the maximum penetration depth can be predicted. Table 5 lists the input factors and their response values for the optimization study, while Table 6 lists the optimization boundary constraints, limits, goals and importance aspects of the design expert software used to do the optimization calculations for the factors studied. The selected effective design parameters in the optimization are the liner wall thickness T_L, the jet kinetic energy, the jet mass (m_j) produced and the calculated penetration depth. The response parameters that will be considered are the penetration depth (to be maximized) and both the jet kinetic energy and the liner mass (to be within the specified range).

Table 5. The input factors and their response values for the optimization study

Liner thickness T_L [mm]	Jet mass m_j [g]	Jet K.E. [kJ]	Calculated P [mm]
0.7	2.31	48.52	88.88
0.8	2.55	47.89	93.14
0.9	2.79	47.20	98.93
1.0	3.05	46.62	103.00
1.1	3.18	45.83	113.64
1.2	3.40	44.80	111.33
1.3	3.59	43.11	109.02

Table 6. The optimization constraints, limits and importance aspects

Parameter	Goal	Lower limit	Upper limit	Importance
m_j [g]	in range	2.31	3.59	+
Jet K.E. [kJ]	in range	43.11	48.52	+
Calculated P [mm]	maximize	88.88	113.64	+++

To illustrate the dependency of the penetration depth on both the jet mass and relevant kinetic energy, both the desirability and the contour of the 3-D penetration curves are shown in Figures 11 and 12, respectively, which are the optimization results obtained using the design expert software. These graphs illustrate areas at which the desirability could be very high and approaches unity. It is seen from Figure 11 that the preferred areas of the highest desirability (*i.e.* close to unity) are represented by red colours, whereas the blue colour area refers to the undesirable area. Any combination between the jet mass and kinetic energy determines the values of the desirability from Figure 11 and the penetration depth from Figure 12 depending on the objective function formed by the input data.

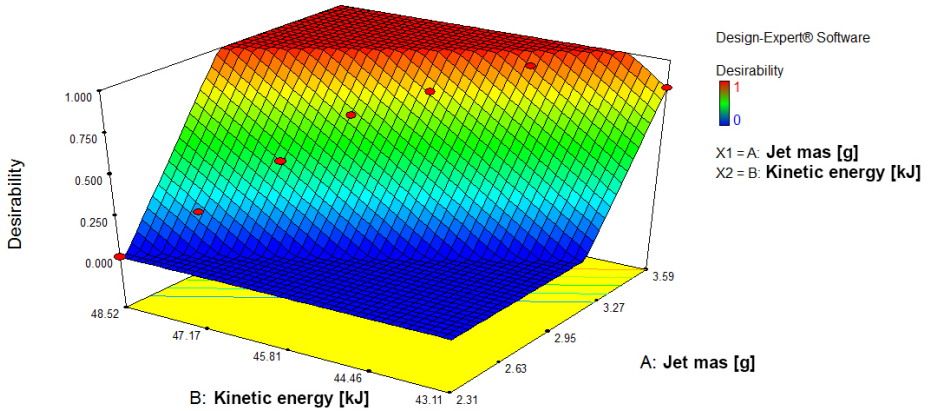

Figure 11. 3-D surface of the calculated desirability for the optimization problem

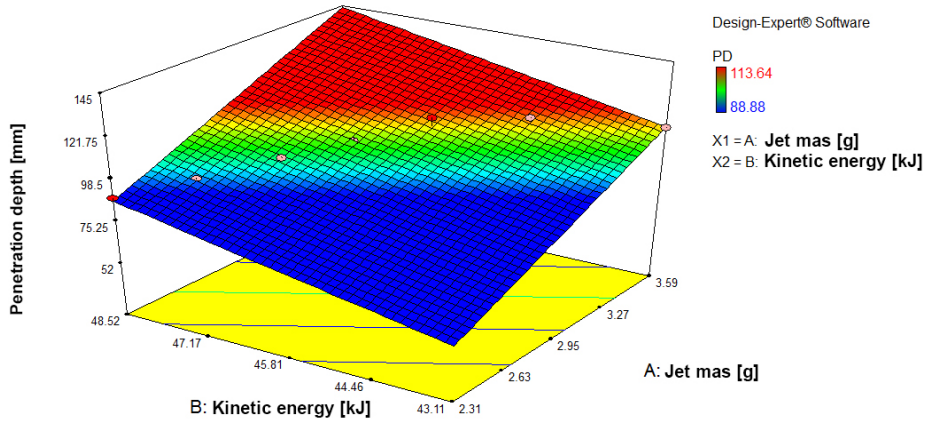

Figure 12. 3-D surface of the calculated penetration depth for the optimization problem

Table 7 lists the results obtained from the optimization run. The five solutions in this table are arranged according to their desirability, which is observed to be almost unity for the whole range. This represents a high degree of accuracy between the expected response calculated by the statistical objective function based on the fitting data of the input factors and that presented as an estimated penetration depth. In general, desirability with zero value represents a completely undesirable response, while the desirability value of unity represents an ideally desirable response [37].

Table 7. The optimization output and the selected, relevant and predicted penetration depth based on design expert software

Number	Liner thickness [mm]	Jet mass [g]	Kinetic energy [kJ]	Penetration depth [mm]	Desirability
1	1.050	3.08	49.44	118.04	1
2	1.055	3.09	49.13	116.93	1
3	1.110	3.15	45.90	114.75	1
4	1.036	3.05	48.37	113.21	1
5	1.026	3.03	47.90	112.44	1
6	1.003	2.98	48.18	111.91	1

Generally, the outputs of the optimization process are arranged in descending order according to the desirability value. The first two values for liner thicknesses of 1.050 and 1.055 were expected to achieve the largest penetration depths. However, the higher values of the kinetic energy needed for both designs should be highlighted. Higher kinetic energy requires more explosive loading, which is not acceptable in our design. On the other hand, increasing the kinetic energy requires increasing the jetting related velocities, which may encounter instability during the early stage of jet formation, *i.e.* the flow velocity of the copper liners should satisfy the stability condition:

$$v_{\text{flow, max}} \leq 1.23 C_o \tag{5}$$

where $v_{\text{flow, max}}$ is the maximum flow velocity from all of the collapsed liner elements and C_o is the sound speed in the copper (C_o = 3940 m/s) [38].

4.5 Comparison between the predicted and measured penetration depths

Figure 13 plots the predicted penetration depth obtained using the virtual origin concept and its dependence on liner thickness. The corresponding measurements of penetration depths are plotted on the same figure. It can be seen in Figure 13 that the predicted penetration depth is a maximum for a liner thickness of 1.1 mm. This depth is slightly less than that predicted by the optimization analysis, which gave an optimum liner wall thickness of 1.05 mm. For liner wall thicknesses ranging from 0.8 to 1.2 mm, the measured penetration depths into steel targets are compared with the corresponding predictions: good agreement was generally obtained. The maximum absolute difference was found to be 13.59% for a liner thickness of 0.8 mm. This may be attributed

to the accuracy of the charge filling process and assembly of the shaped charge elements in addition to the ductility of the used copper material. The ductility has an important role in increasing the breakup time of jets, which in turn affects the resulting penetration depth. Typical images of the measured penetration depths of shaped charge jets formed from liner thicknesses of 0.8-1.2 mm into steel targets can be seen in Figure 14.

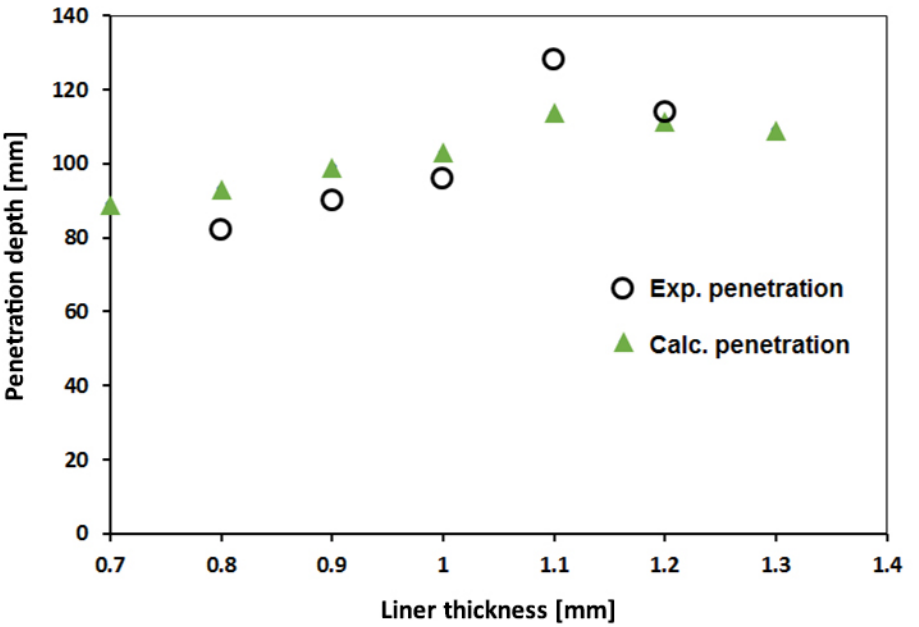

Figure 13. Comparison between predicted penetration depth and corresponding measurement for each liner thickness of the shaped charges used

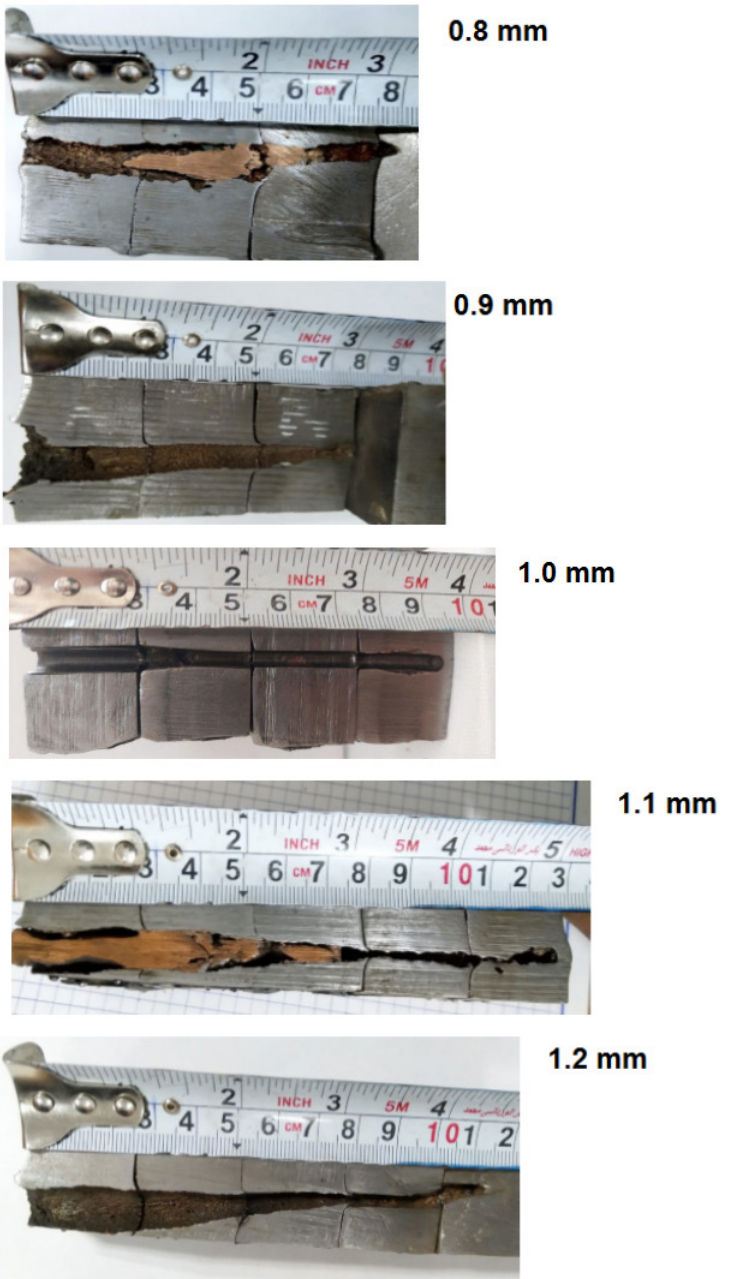

Figure 14. Typical views of the jet penetration depths into steel targets for liner thicknesses of 0.8, 0.9, 1.0, 1.1 and 1.2 mm

It can be seen from the measured depths that the penetration of a jet is very sensitive to its ductility and particulation as well as the jet drift phenomena. Another crucial parameter that has a significant influence on the measured penetration depth is the flow velocity of the collapsed liner element; V_{flow}, as discussed in Section 4.4 [39].

The maximum predicted flow velocities were calculated to be 4960 and 4560 m/s for liner thicknesses of 1.0 and 1.1 mm, respectively, which means that the jet produced from a liner with a thickness of 1 mm is non-coherent during its stretching. This accounts for the liner thickness of 1.1 mm, which is considered to be the maximum instead of the 1 mm-thickness liner. The coherency criterion has been confirmed by the measured penetration depths shown in Figure 14, where the maximum penetration depth is obtained from the shaped charge design having a liner thickness of 1.1 mm. This design achieved a penetration depth of more than 12 cm in a steel target despite all the drawbacks due to manual loading and assembly as well as testing of shaped charge designs that have a negative effect on penetration.

It could be concluded that shaped charges with a liner thickness of 1.1 mm may give better performance when automatic loading (filling) of the explosive is applied. It could also give a very large promising penetration when more powerful explosives with higher detonation velocity (such as HMX-based PBXs) that can be pressed during loading instead of extruded or cast.

5 Conclusions

- The effect of shaped charge liner wall thickness on the penetration depth into a laminated steel target was investigated both experimentally and numerically. An experimental program was performed to construct and test the shaped charge jets formed from different liner thicknesses against steel targets. An Autodyn hydrocode was used to predict the jetting analysis data necessary for applying the virtual origin concept. The main conclusions of the present research are summarized as follows:
- Both the jet mass and its kinetic energy have a significant effect on the predicted penetration depth. An optimization study using design expert optimization software indicates that the optimum liner wall thickness that achieves the maximum penetration depth into steel target lies between 1.0 and 1.1 mm.
- A liner thickness of 1.1 mm achieved the greatest measured penetration depth into steel targets. An analytical study excluded liner thicknesses of 1.0 mm

due to their non-coherent flow velocity, which exceeds the threshold coherent velocity limit.

- The maximum absolute error between the measured and the predicted penetration depths was found to be 13.59% for a liner thickness of 0.8 mm, which may be attributed to the manual filling and assembly process of the shaped charges.

References

[1] Walters, P.; Zukas, J. *Fundamentals of Shaped Charge.* John Wiley & Sons, **1989**; ISBN-10: 0471621722.
[2] Elshenawy, T.; Elbeih, A.; Li, Q.M. Influence of Target Strength on the Penetration Depth of Shaped Charge Jets into RHA Targets. *Int. J. Mech. Sci*. **2018**, *136*: 234-242.
[3] Elshenawy, T.; Li, Q. Influences of Target Strength and Confinement on the Penetration Depth of an Oil Well Perforator. *Int. J. Impact Engineering* **2013**, *54*: 130-137.
[4] Voitenko, Y.I.; Zakusylo, R.V.; Wojewódka, A.T.; Gontar, P.A.; Gerlich, M.M.; Drachuk, O.G. New Functional Materials in Mechanical Engineering and Geology. *Cent. Eur. J. Energ. Mater.* **2019**, *16*(1): 135-149.
[5] Voitenko, Y.; Zakusylo, R.; Zaychenko, S. Influence of the Striker Material on the Results of High-Speed Impact at a Barrier. *Cent. Eur. J. Energ. Mater.* **2021**, *18*(3): 405-423.
[6] Nan, Y.X.; Jiang, J.W.; Wang, S.Y.; Men, J.B.; Chen, D.P. Penetration Capability of Shaped Charge Loaded with Different High-energy Explosives. *Proc. 28th Int. Symp. Ballistics*, **2014**.
[7] Saran, S.; Ayısıt, O.; Yavuz, M.S. Experimental Investigations on Aluminium Shaped Charge Liners. *Procedia Eng.* **2013**, *58*: 479-486.
[8] Dehestani, P.; Fathi, A.; Daniali, H.M. Numerical Study of the Stand-off Distance and Liner Thickness Effect on the Penetration Depth Efficiency of Shaped Charge Process. *Proc. Inst. Mech. Eng., Part C,* **2019**, *233*(3): 977-986.
[9] Ou, J.H.; Jen-Bing, O.; Yan-Jing, J. The Design and Analysis for Shaped Charge Liner Using Taguchi Method. *Int. J. Mechanics*. **2014**, *8*: 53-61.
[10] Fujiwara, S.; Abiko, K. Ductility of Ultra High Purity Copper. *Le Journal de Physique IV*, **1995**. *5*: C7/295-300.
[11] Held, M. Liners for Shaped Charges. *J. Battlefield Technol*. **2001**, *4*(3): 1-6.
[12] Elbeih, A.; Zeman, S.; Jungová, M.; Akštein, Y.; Vávra, P. Detonation Characteristics and Penetration Performance of Plastic Explosives. *Proc. Int. Autumn Semin. Propellants, Explos. Pyrotech.: Theory Pract. Energ. Mater.*, China, **2011**, 508-13.
[13] Sućeska, M. EXPLO5 – Computer Program for Calculation of Detonation Parameters. *Proc. of 32nd Int. Annual Conf. ICT*, Karlsruhe, Germany, **2001**, 110/1-13.

[14] Peter, X.K.; Jiba, Z.; Olivier, M.; Snyman, I.M.; Mostert, F.M.; Sono, T.J. Prediction of Detonation and JWL EOS Parameters of Energetic Materials Using EXPLO5 Computer Code. *Proc. South African Ballistic Organization,* Cape Town, South Africa, **2016**.
[15] Vasilescu, G.; Kovacs, A.; Gheorghiosu, E.; Garaliu, B.; Ilcea, G. Numerical Simulation for Determining Detonation Parameters of Explosive Substances Using EXPLO5 Thermo-chemical Prediction Software. *MATEC Web of Conferences,* **2020**, *305*, p. 00049.
[16] *MatWeb, Material Property Data.* Mitsubishi Chemical Advanced Materials, **2021**, http://www.matweb.com/
[17] Malcolm, S. *Autodyn Theory Manual*. Century Dynamics, CA, **1997**.
[18] Johnson, G.R.; Cook, W.H. A Constitutive Model and Data for Metals Subjected to Large Strains, High Strain Rates and High Temperatures. *Proc. 7th Int. Symp. Ballistics,* the Hague, the Netherlands, **1983**, 541-547.
[19] Couque, H.; Boulanger, R.; Bornet, F. A Modified Johnson-Cook Model for Strain Rates Ranging from 10^{-3} to 10^{5} s^{-1}. *J. Phys. IV France* **2006**, *134*: 87-93.
[20] Tarver, C.M.; Tao, W.C.; Lee, C.G. Sideways Plate Push Test for Detonating Solid Explosives. *Propellants Explos. Pyrotech*. **1996**, *21*(5): 238-246.
[21] Lan, I.F.; Hung, S.C.; Chen, C.Y.; Niu, Y.M.; Shiuan, J.H. An Improved Simple Method of Deducing JWL Parameters from Cylinder Expansion Test. *Propellants Explos. Pyrotech*. **1993**, *18*(1): 18-24.
[22] Elek, P.M.; Džingalašević, V.V.; Jaramaz, S.S.; Micković, D.M. Determination of Detonation Products Equation of State from Cylinder Test: Analytical Model and Numerical Analysis. *Therm. Sci.* **2015**. *19*(1): 35-48.
[23] Kato, H.; Kaga, N.; Takizuka, M.; Hamashima, H.; Itoh, S. Research on the JWL Parameters of Several Kinds of Explosives. *Mater. Sci. Forum* **2004**, *465-466*: 271-276.
[24] Birkhoff, G.; MacDougall, D.P.; Pugh, E.M.; Taylor, S.G. Explosives with Lined Cavities. *J. Appl. Phys*. **1948**, *19*(6): 563-582.
[25] Pugh, E.M.; Eichelberger, R.J.; Rostoker, N. Theory of Jet Formation by Charges with Lined Conical Cavities. *J. Appl. Phys*. **1952**, *23*(5): 532-536.
[26] Elshenawy, T.; Elbeih, A.; Li, Q.M. A Modified Penetration Model for Copper-Tungsten Shaped Charge Jets with Non-uniform Density Distribution. *Cent. Eur. J. Energ. Mater*. **2016**, *13*(4): 927-943.
[27] Malcolm, S. *Autodyn Jetting Tutorial, R. 3.0. Editor.* Century Dynamics, US. **1997**.
[28] Gürel, E. Modeling and Simulation of Shaped Charges. Master dissertation, Middle East Technical University, **2009**.
[29] Elshenawy, T.; Elbeih, A.; Klapötke, T.M. A Numerical Method for the Determination of the Virtual Origin Point of Shaped Charge Jets Instead of Using Flash X-ray Radiography. *J. Energ. Mater*. **2018**, *36*(2): 127-140.
[30] Chou, P.C.; Flis, W.J. Recent Developments in Shaped Charge Technology. *Propellants, Explos. Pyrotech*. **1986**, *11*(4): 99-114.

[31] Aseltine, C.L. *Analytical Predictions of the Effect of Warhead Asymmetries on Shaped Charge Jets*. Army Ballistic Research Lab, Aberdeen Proving Ground MD, Report No. ARBRL-TR-02214, **1980**.
[32] Hirsch, E. Scaling of the Shaped Charge Jet Break-Up Time. *Propellants Explos. Pyrotech*. **2006**, *31*(3): 230-233.
[33] Elshenawy, T.; Li, Q.M. Breakup Time of Zirconium Shaped Charge Jet. *Propellants Explos. Pyrotech*. **2013**, *38*(5): 703-708.
[34] Allison, F.E.; Vitali, R. *A New Method of Computing Penetration Variables for Shaped Charge Jets*. Aberdeen Proving Ground, Ballistic Research Lab., Report No 1184, Maryland, **1963.**
[35] DiPersio, R.; Simon, J.; Merendino, A. *Penetration of Shaped-charge Jets into Metallic Targets*. Aberdeen Proving Ground, Ballistic Research Lab., Report No 1296, Maryland, **1965**.
[36] Schwartz, W. Modified SDM Model for the Calculation of Shaped Charge Hole Profiles. *Propellants Explos. Pyrotech*. **1994**, *19*(4): 192-201.
[37] *Design-Expert Software.* StatEase®, **2020**, https://www.statease.com/software/design-expert.
[38] Hasenberg, D. *Consequences of Coaxial Jet Penetration Performance and Shaped Charge Design Criteria*. Naval Postgraduate School, Report NPS-PH-10-001, Monterey, CA, US, **2010**.
[39] Elshenawy, T.; Li, Q.M.; Elbeih, A. Experimental and Numerical Investigation of Zirconium Jet Performance with Different Liner Shapes Design. *Def. Technol.* **2022**, *18*: 12-26.

Received: September 29, 2021
Revised: March 24, 2022
First published online: March 31, 2022